



Anodising of 2024-T3 aluminium alloy in electrolyte of sulphuric–boric–phosphoric mixed acid containing cerium salt as corrosion inhibitor

Mohsen SAEEDIKHANI, Mehdi JAVIDI, Sareh VAFAKHAH

Department of Materials Science and Engineering, School of Engineering,
Shiraz University, Zand Street, Shiraz 7134851154, Iran

Received 13 February 2016; accepted 23 December 2016

Abstract: The effect of cerium salt as an inhibitor in anodising of the 2024-T3 aluminium alloy was studied. Scanning electron microscopy equipped with energy dispersive X-ray spectroscopy was used to study the surface composition of the alloy before and after surface preparation. A mixed electrolyte of 10% sulphuric acid, 5% boric acid and 2% phosphoric acid containing 0.1 mol/L cerium sulphate salt was used as the anodising electrolyte. Sealing treatment was also done in boiling water and molten stearic acid. Electrochemical impedance spectroscopy and salt spray techniques were performed in order to investigate the corrosion behaviour and durability of the oxide films, respectively. It was concluded that the presence of cerium ions in anodising electrolyte resulted in the increase in homogeneity, the rate of oxide film growth and also the thickness of the oxide layer, owing to the high oxidising power of cerium ion.

Key words: aluminium alloy; anodising; mixed acid; cerium salt; inhibitor

1 Introduction

Aluminium alloys containing copper (2000 series) exhibit high strength and are widely used in the aviation industry but generally they show low corrosion resistance and are susceptible to localized corrosion. Also, intermetallic particle phases which give strength to these alloys could result in the susceptibility of the alloys to galvanic corrosion [1,2]. Thus, these alloys are mostly anodised to improve their corrosion resistance.

The application of an anodic polarization to an aluminium alloy sample which is immersed in an appropriate electrolyte leads to anodic oxide film growth [3]. This film is most often characterised by a duplex structure composed of an inner thin barrier layer and a thick outer porous layer. Anodising of aluminium alloys in chromic acid electrolytes was common which now is prohibited since Cr (VI) is toxic and carcinogenic. There is not only a sole candidate for the replacement of Cr(VI) in anodising electrolyte [4] thus most researchers have focused their investigation on the combination of different techniques to improve corrosion resistance of oxide film such as using mixed-acid-electrolyte [3,5,6]. In our previous work [3], we studied the anodising

process of 2024-T3 aluminium alloy in sulphuric–boric–phosphoric mixed acid electrolyte. It was concluded that the use of mixed acidic electrolyte provides reasonable corrosion resistance for the 2024-T3 alloy.

MOUTARLIER et al [7–9] proposed acid baths containing rare earth corrosion inhibitors as the substitute for chromic acid in anodising bath in term of improving corrosion resistance. They used sulphuric acid bath containing molybdate ion and cerium IV ion species. Rare earth elements like cerium, hafnium and neodymium have been used in the anodising process of aluminium by several ways including treatment of aluminium before anodising (surface preparation); after anodising (sealing process) and also as one of the anodising electrolyte species. Cerium ions act as a cathodic inhibitor on intermetallic particles of aluminium alloy structure. Cerium oxide and/or cerium hydroxide precipitate(s) in response to increase of pH on the surface of cathodic particles as the alloy briefly corrodes after immersing in corrosive media. The precipitates prevent further corrosion by hindering the reduction of oxygen and water [10].

The corrosion resistance of anodised aluminium alloys could be enhanced by a hydrothermal treatment named sealing. Researchers have reported different

sealing methods for aluminium oxide film [3,11–14]. The early method is sealing in boiling water, which improves the corrosion resistance of anodised alloys. The sealing of anodic films effectively prevents the risk of pitting corrosion even in high corrosive environments. The main role of sealing process is blockage of the pores [9].

Electrochemical techniques have been employed to study the corrosion resistance of anodised aluminium alloys. Electrochemical impedance spectroscopy (EIS) technique could characterise the properties of the barrier layer and the sealed porous layer by fitting the impedance spectra to an appropriate electrical equivalent circuit. The resulted electrochemical data from EIS technique could also be used for calculation of the thickness of oxide films [15].

In this study, we have modified our proposed sulphuric–boric–phosphoric mixed acid bath [3] with cerium(IV) ion as a corrosion inhibitor for the anodising process of the 2024-T3 alloy. Cerium salts likewise cerium cinnamate [16], cerium tartrate [17] and cerium sulphate (in present work) have reasonable corrosion inhibition action on the 2024-T3 aluminium alloy. The corrosion behaviour of the anodised alloy and also the degradation of oxide film were investigated in an aggressive medium using electrochemical impedance spectroscopy. The durability of the anodised alloy was evaluated by employing salt spray technique.

2 Experimental

2.1 Materials

The investigated material was a 2024-T3 aluminium alloy whose chemical composition was analyzed using an optical emission spectrometer (OES). Scanning electron microscopy (SEM) and energy dispersive X-ray spectroscopy (EDS) methods (VEGA II TESCAN trademark) were employed to study the surface composition of the alloy before and after surface preparation both before anodising process.

2.2 Surface preparation

The surfaces of the samples were wet ground up to 800 grit SiC abrasive papers and cleaned with deionized water and acetone. The samples were alkaline cleaned, chemically polished and finally de-smutted. After each step, the samples were rinsed with deionized water and air dried. Table 1 lists the chemical composition of the solutions used for surface preparation and their related holding time and temperature.

2.3 Anodising and sealing

A mixed electrolyte with the composition of 10% sulphuric acid, 5% boric acid and 2% phosphoric acid

containing 0.1 mol/L of cerium sulphate was used as the anodising electrolyte. All the acids used in this research and cerium sulphate salt ($\text{CeSO}_4 \cdot 4\text{H}_2\text{O}$) were analytical grade and prepared from Merck. A simple rectifier with a maximum power output of 40 V and 4 A was employed for applying anodic polarization. Anodising process was carried out at room temperature under the current density of 1 mA/cm² for 20 min. An enough large lead sheet was used as a cathode, and the prepared 2024-T3 alloy was the anode with dimensions of 2 mm × 10 mm × 50 mm. Sealing treatment was performed in boiling water and also in molten stearic acid at 90 °C both for 30 min. Finally, the samples were rinsed, and air dried.

Table 1 Chemical composition of solutions used for surface preparation and their holding time and temperature

Surface preparation	Chemical composition of solution	Temperature/ °C	Time/ min
Alkaline cleaning	12 g NaOH + 100 mL H ₂ O	60	3
Chemical polishing	54 mL H ₃ PO ₄ (85%) + 2 mL HNO ₃ (66.4%)+ 15 mL CH ₃ COOH (99%)+ 13 mL H ₂ O	90	4
Deoxidizing	35 mL HNO ₃ (66.4%)+ 65 mL H ₂ O	26	2

2.4 Electrochemical and salt spray testing

The corrosion behavior of the anodised alloys was studied, and EIS technique was employed with three-electrode configuration cell. A saturated Ag/AgCl (saturated, KCl 3 mol/L) electrode as the reference electrode, a platinum rod as an auxiliary electrode and the anodised sample as working electrode were employed. The electrochemical test cell was open to air at room temperature containing aqueous electrolyte of 3.5% NaCl solution. The samples were dipped in the electrolyte for 1, 2, 10, 24 and 48 h to study the degradation of the oxide film. Impedance measurements were taken over a frequency range of 1.0×10^5 down to 1.0×10^{-2} Hz using a 10 mV single sine wave. Data were shown as Nyquist and Bode plots. The equipment for electrochemical tests was μ Autolab typeIII with the frequency response analyser (FRA) software for analyzing the resulted EIS spectrum.

Neutral salt spray testing was performed according to ASTM B117 standard during which the anodised samples were exposed to 3.5% NaCl solution at 35 °C.

3 Results and discussion

3.1 Surface preparation

The bulk chemical composition of the investigated

alloy which resulted from optical emission spectrometer is listed in Table 2. Copper is one of the most important alloying elements for 2024-T3 alloy due to its strengthening effect. Furthermore, the 2024-T3 alloy contains other alloying elements which lead to the presence of several intermetallic phases in the structure [8].

Table 2 Bulk chemical composition of 2024-T3 aluminium alloy (mass fraction, %)

Cu	Mg	Mn	Fe	Zn	Si	Others	Al
4.62	1.55	0.57	0.18	0.15	0.1	0.04	Bal.

The SEM image of the surface of the 2024-T3 alloy is shown in Fig. 1(a) which illustrates the presence of different particles. The EDS analysis of the surface of the 2024-T3 alloy reveals that the dark areas correspond to Al–Cu–Mg particles, and the white areas correspond to Al–Cu–Mn–Fe–Si particles. It can be seen from Fig. 1(a) that Al–Cu–Mg particles have nearly round shape, and Al–Cu–Mn–Fe–Si particles have irregular shape. In order to prevent damaging of the alloy surface (by dissolving copper containing particles) during anodising

process, the surface of the alloy should be depleted from copper/copper-containing phases. Alkaline cleaning, chemical polishing and deoxidizing solutions were employed to treat the surface of the alloy before anodising.

During alkaline cleaning, lots of gases were emitted from the alloy surface and after alkaline cleaning the alloy surface was covered with black smuts which may be metal oxides or hydroxides such as silicon and copper dust. The smuts were completely removed during chemical polishing. After chemical polishing, it was seen that a thin layer with cuprous colour formed on the alloy surface, probably due to leaching of copper from the surface of the alloy. This layer was easily removed by washing in the deionized water stream. After chemical polishing, the deoxidizing process was performed. The surface treated alloy was chemically analyzed to ensure that bulk chemical composition of the alloy remained unchanged during chemical polishing.

Table 3 lists the bulk chemical composition of the alloy after surface treatment, resulted from OES technique. It can be seen that there is no significant change in the bulk chemical composition of the alloy.

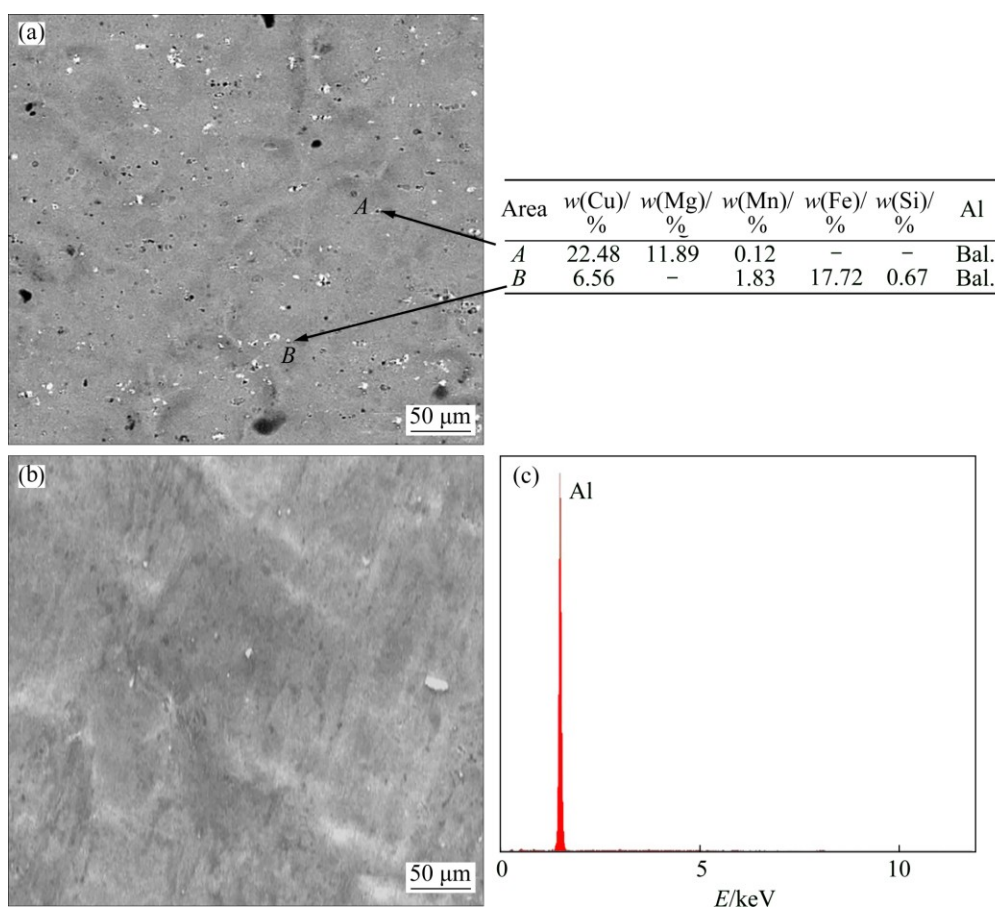


Fig. 1 SEM images of surface of 2024-T3 aluminium alloy before surface treatment and corresponding EDS analysis of surface of alloy (a), SEM image of 2024-T3 aluminium alloy after surface treatment (b), EDS analysis on surface of alloy after surface treatment (c) [3]

Table 3 Bulk chemical composition of 2024-T3 aluminium alloy after surface treatment (mass fraction, %)

Cu	Mg	Mn	Fe	Zn	Si	Others	Al
4.45	1.57	0.56	0.17	0.16	0.06	0.04	Bal.

Figure 1(b) shows the SEM image of the alloy after surface treatment. EDS analysis of the surface revealed that no other element is present on the alloy surface except aluminum, as can be concluded from the resulted EDS spectra shown in Fig. 1(c).

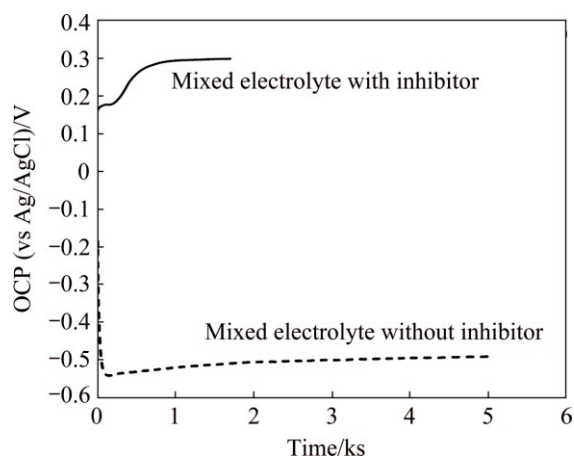
It should be noted that copper can exist in two valence states of Cu^+ and Cu^{2+} , thus possibly permitting electron switching. Its presence in oxide film increases the electronic conductivity of the oxide film. Thus, eliminating of copper or intermetallic phases which contain copper from the alloy surface before anodising, as done in this study, decreases the probability of the presence of copper in the oxide film.

3.2 Electrochemical study of anodised alloy

The resulted anodic oxide film obtained from the proposed electrolyte was uniform and relatively smooth. Generally, the aluminum oxide film consists of an inner thin barrier layer and a thick outer porous layer. Also, the porous part is composed of pores and walls of hexagonal cells [9].

3.2.1 Open circuit potential

The variation of open circuit potential (OCP) of 2024-T3 alloy in the mixed acid electrolyte with and without Ce(IV) inhibitor is shown in Fig. 2. In the mixed-electrolyte without inhibitor, it can be seen that OCP of the alloy reaches a steady value (-0.51 V vs Ag/AgCl) after a relatively large time of almost 5000 s. On the other hand, in the mixed-electrolyte containing Ce(IV) as the corrosion inhibitor, the OCP of the alloy increased rapidly in the initial period which is due to the high oxidizing power of cerium ion. The OCP reached a

**Fig. 2** Variations of OCP of 2024-T3 alloy in mixed electrolyte with and without inhibitor

steady noble value of +300 mV in a period of fewer than 1800 s. The shift of OCP toward noble potentials is attributed to the formation of alumina layer. MOUTARLIER et al [8] reported that dissolution of Cu-rich phases occurs during anodising of 2024 alloy in acidic electrolytes. The alloy was immersed in the mixed electrolyte containing 0.1 mol/L Ce(IV) ion as the corrosion inhibitor for 1800 s just before anodising. This process resulted in shifting up the electrode potential to +300 mV (vs Ag/AgCl) which is much higher than the dissolution potential of copper (39 mV vs Ag/AgCl) [8]. Thus, dissolution of copper would be hindered during anodising.

3.2.2 Electrical equivalent circuit

In order to investigate the EIS parameters of the anodic film, barrier and porous layers were considered as two separate oxide phases and independent with each other. The electronic and dielectric properties of each oxide phase can be studied by proposing an electrical equivalent circuit composed of parallel and series resistances and capacitances. Each part of the aluminium oxide film (i.e., pore, barrier layer and wall of hexagonal cells) has both capacitive and resistive behaviour and thus the oxide film can be modelled by a circuit shown in Fig. 3(a).

Several authors [5,9] reported that the circuit proposed in Fig. 3(a) successfully explains the properties of both oxide parts. In this model, R_5 is the resistance of 3.5% NaCl aqueous solution with the approximate extent of $15 \Omega \cdot \text{cm}^2$. Furthermore, R_3 and CPE3 represent the wall of hexagonal cells and they were eliminated from the circuit because they are extremely high and extremely low, respectively [9]. Thus, the passage of electrical current is prevented through the wall of hexagonal cells and the model is reduced to the model as shown in Fig. 3(b).

Thus, the EIS parameters concerning anodic oxide film are R_1 as porous layer resistance, CPE1 as porous layer constant phase element, R_2 as barrier layer resistance and CPE2 as barrier layer constant phase element. The capacitive behaviour of the barrier and porous layers is well simulated by constant phase elements (CPE) than by a pure capacitance (C) because of their inhomogeneity. The use of CPE usually increases the goodness of the fit and in studies of corroding systems, CPE is most often used to describe the frequency dependence of non-ideal capacitive behaviour [3, 9]. The impedance of a CPE (Z_{CPE}) is given by

$$Z_{\text{CPE}} = Q^{-1}(j\omega)^{-n} \quad (1)$$

where Q corresponds to the capacitive behaviour, parameter n is frequency dispersion factor which depends on different factors such as surface roughness [9]

and varies from 0 to 1. The more homogeneous the surface is, the smoother the surface is, and thus parameter n has a closer value to 1. When n is equal to 1, parameters CPE1 and CPE2 can be considered as ideal capacitances. The method proposed by MANSFELD et al [18,19] was used in order to convert CPE to C.

3.2.3 EIS study of unsealed anodised alloy

The alloy was immersed in sulphuric-boric-phosphoric acid electrolyte containing 0.1 mol/L cerium ion for 1800 s then immediately anodised for 20 min under a current density of 1mA/cm². The Nyquist plot of the anodised alloy is shown in Fig. 4(a), and related EIS parameters are shown in Table 4. The porous layer could not be characterized when the oxide film is unsealed because of the high conductivity of the pores which filled with the brine solution. Therefore, one capacitive loop is observed in low frequency range which is related to the barrier layer.

By comparing the data reported in Table 4, it can be

concluded that EIS parameters (and also corrosion resistance) of the anodised film were improved by adding cerium ion to the electrolyte. As can be seen, the capacitance of the barrier layer is decreased from 0.57 $\mu\text{F}/\text{cm}^2$ to 0.48 $\mu\text{F}/\text{cm}^2$ and also both of the n_2 and R_2 are increased. As it was mentioned before, Al–Cu–Mg phases are anodic relative to the aluminium matrix. Addition of cerium ions to anodising electrolyte leads to the formation of hydroxide deposits on Al–Cu–Mg phases [20]. These hydroxide precipitates could act as diffusion barrier retarding the anodic reactions on these phases and increasing the corrosion resistance.

A corrosion resist oxide film has a low value of capacitance and a large value of resistance. A capacitance with lower capacity consumes less electrical current to be charged. Current means flow of electrons via charge transfer in corrosion of aluminium. When a capacitance is charged, no more current will pass through it. Thus, the sooner a capacitance being charged, the sooner

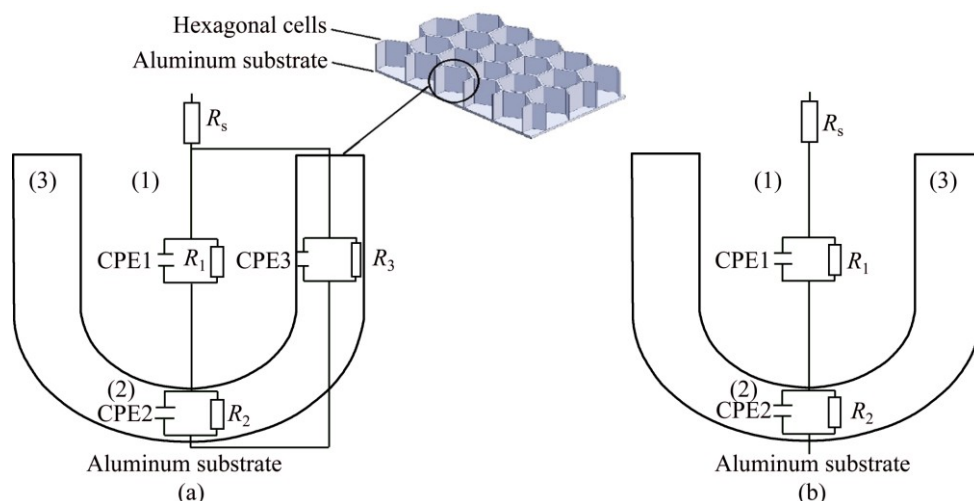


Fig. 3 Electrical equivalent circuit for modelling impedance behaviour of alumina film (a) and simplified model (b) for equivalent circuit shown in (a): 1—Pores of porous layer, CPE1—Porous layer constant phase element, R_1 —Porous layer resistance; 2—Barrier layer, CPE2—Barrier layer constant phase element, R_2 —Barrier layer resistance; 3—Walls of hexagonal cells, CPE3—Hexagonal cells constant phase element, R_3 —Hexagonal cells resistance

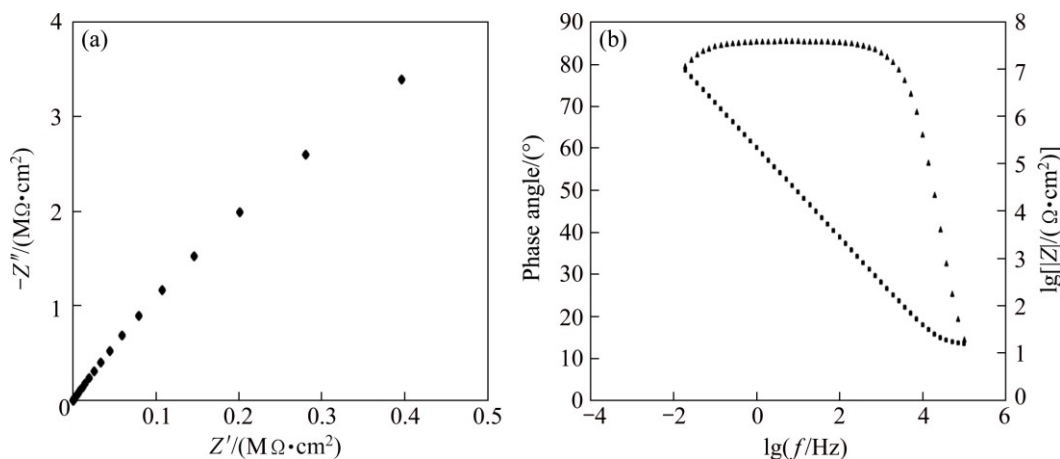


Fig. 4 Nyquist plot (a) and Bode phase and bode magnitude plot (b) of unsealed anodised alloy

Table 4 EIS parameters of barrier and porous layers for anodic oxide film

Anodising process	Sealing	Layer	$C/$ ($\mu\text{F}\cdot\text{cm}^{-2}$)	$R/$ ($\Omega\cdot\text{cm}^2$)	n
Anodising in mixed acid [3]	Unsealed	Barrier layer	0.57	6.5×10^6	0.92
	Unsealed	Barrier layer	0.48	9×10^7	0.95
Anodising in mixed acid containing 0.1 mol/L cerium sulphate	Sealed in boiling Water	Barrier layer	0.21	1.4×10^9	0.98
	Sealed in molten stearic acid	Porous layer	0.25	3×10^5	0.93
		Barrier layer	0.18	2.1×10^{10}	0.98
		Porous layer	0.22	4.8×10^6	0.95

the current passage will be disconnected through it. Considering both capacitive and resistive behaviour of the oxide film, the other path for current passage is through resistance. Higher values of resistance result in higher resistance against current passage and corrosion. Thus, this is the way that coatings with the lower value of capacitance and higher value of electrical resistance provide better corrosion resistance.

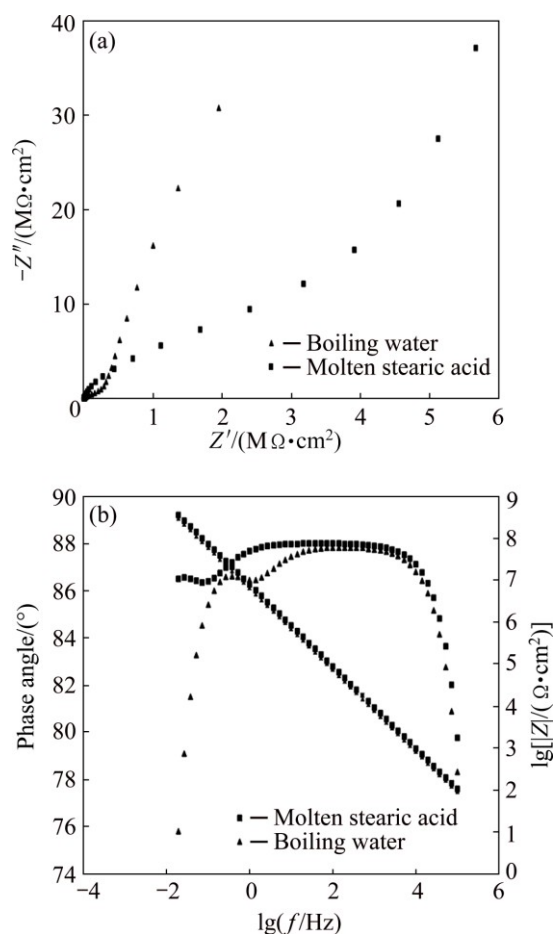
An increase in the value of n for barrier layer indicates the effective role of cerium inhibitor in increasing the homogeneity of the oxide film.

The Bode phase and Bode magnitude plots of the unsealed anodised alloy are also shown in Fig. 4(b). The single inflection point in Bode phase plot and also the single slope in the Bode magnitude plot indicate that there exists only one time constant in the impedance spectra and also confirm the single capacitive loop of the related Nyquist plot in Fig. 4(a). The slope of the Bode magnitude plot is determined by the ratio of R_2 to R_s in Fig. 2(a). In general, the slope approaches to -1 as this ratio increases. It can be seen from Fig. 4(b) that the phase angle of the barrier layer is almost near to 90° in a frequency range of approximately 0.01 Hz up to 1000 Hz which corresponds to the pure capacitive impedance behaviour of the barrier layer.

3.2.4 EIS study of sealed anodised alloy

The sealing process of the anodised alloy was performed in boiling water and molten stearic acid. The Nyquist plots of the sealed anodised alloys are shown in Fig. 5(a). The Nyquist plots of sealed anodised films are characterized by two capacitive loops where the high and medium frequency ranges correspond to sealed porous layer and the low frequency range corresponds to barrier layer. Thus, sealing process enables us to investigate the EIS parameters of porous layer.

By comparing the resulted data in Table 4 it can be

**Fig. 5** Nyquist plot (a) and Bode phase and Bode magnitude plots (b) of sealed anodised alloys by different sealants

concluded that sealing process results in improving in corrosion resistance of the anodic film. Also, an increase in the value of n reveals that the surface becomes much more homogenous after sealing. The micro-pores of alumina layer are physically filled and blocked by boehmite and aluminium hydroxide via sealing in boiling water [12]. Therefore, diffusion of corrosive species like chloride ions, oxygen and water is hindered by pores closure and restricting their access to the alloy surface. On the other hand, an aluminium soap layer forms on the alumina surface after sealing in stearic acid at 90°C [12]. This layer is hydrophobic so repels water and prevents penetrating of corrosive media through the oxide film.

The Bode phase and Bode magnitude plots of the sealed anodised alloys are also shown in Fig. 5(b). Two inflection points and two slopes are observed in Bode phase and Bode magnitude plots, respectively, which correspond to barrier and porous layers and also it is in agreement with the existence of two capacitive loops in the Nyquist plot shown in Fig. 5(a).

The capacitance C_2 can be connected to the barrier layer thickness d_2 , by the use of Eq. (2).

$$C_2 = \varepsilon_0 \varepsilon_r A / d_2 \quad (2)$$

where $\varepsilon_0 = 8.85 \times 10^{-14}$ F/cm is the dielectric constant of vacuum, $\varepsilon_r = 10$ is the relative constant for alumina and A is the electrode surface area. Equation (2) is acceptable when parameter n is close to 1, i.e., the CPE is close to an ideal capacitance. The calculated thickness of the barrier layer for sealed and unsealed oxide layers are reported in Table 5.

Table 5 Thickness of resulted barrier layer for sealed and unsealed oxide layers

Sample	Thickness of barrier layer/nm
Unsealed oxide layer	18
Sealed in boiling water	42
Sealed in molten stearic acid	49

From Table 5 it is evident that sealing process impressively has increased the thickness of the barrier layer which results in improving the corrosion resistance of anodised alloy via blockage of the pores. Also, increase in thickness of barrier layer is more significant in the case of sealing in molten stearic acid than sealing in boiling water. A comparison was made between these data and the reported data for the thickness of the barrier layer in our previous work [3] in which anodising process was performed in sulphuric–boric–phosphoric acid bath without adding cerium ion. In the previous work, the thicknesses of the barrier layer for the unsealed and sealed oxide layer were reported to be 15 nm and 20 nm, respectively. By comparing these data with the data reported in Table 5, it can be concluded that addition of cerium ion to the anodising electrolyte led to increasing the thickness of the barrier oxide layer owing to the high oxidizing power of cerium ion. As it was mentioned before cerium ions act as a cathodic inhibitor at intermetallic particles which are present in the structure of the alloy. Cerium oxide and/or cerium hydroxide precipitate(s) in response to the increase of pH at cathodic particles as the alloy corrodes after being immersed in the corrosive media. The precipitates prevent further corrosion by hindering the reduction of oxygen and water [10] and this might be the way that cerium has increased the corrosion resistance of 2024 alloy in the present work compared with our previous work [3]. On the other hand, DABALA et al [21] proposed that cerium retards both anodic and cathodic reactions.

3.2.5 Immersion testing of sealed anodised alloys

In order to investigate the deterioration rate of the anodised samples sealed in boiling water, they were immersed in 3.5%NaCl aqueous solution from 1 up to 48 h. After immersing, EIS measurements were performed and the resulted data are presented in Fig. 6. For proper

illustration of figures, the impedance spectra are broken into two parts: high and medium frequency range and low frequency range which are related to porous and barrier layers, respectively. The related EIS parameters of the porous and barrier layers are presented in Table 6.

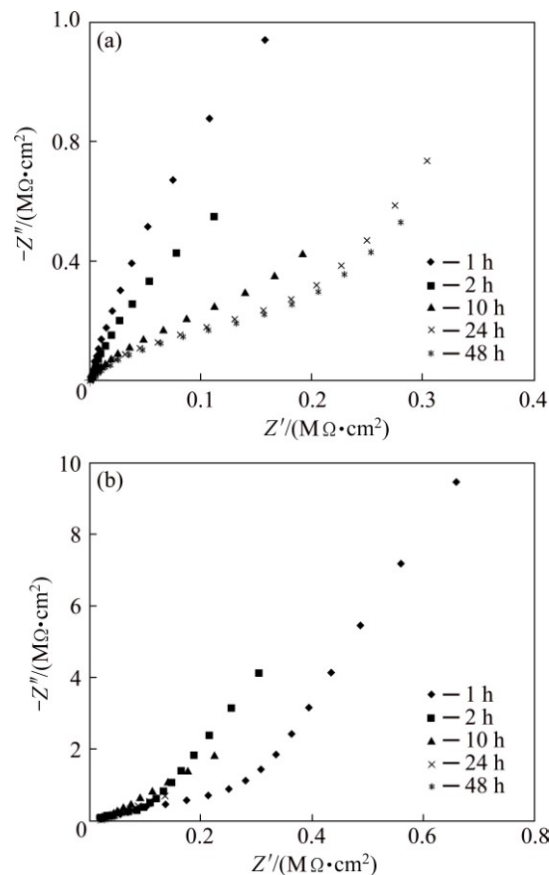


Fig. 6 Nyquist plots after immersion testing for anodised sample sealed in boiling water: (a) High and medium frequency range corresponding to porous layer; (b) Low frequency range corresponding to barrier layer

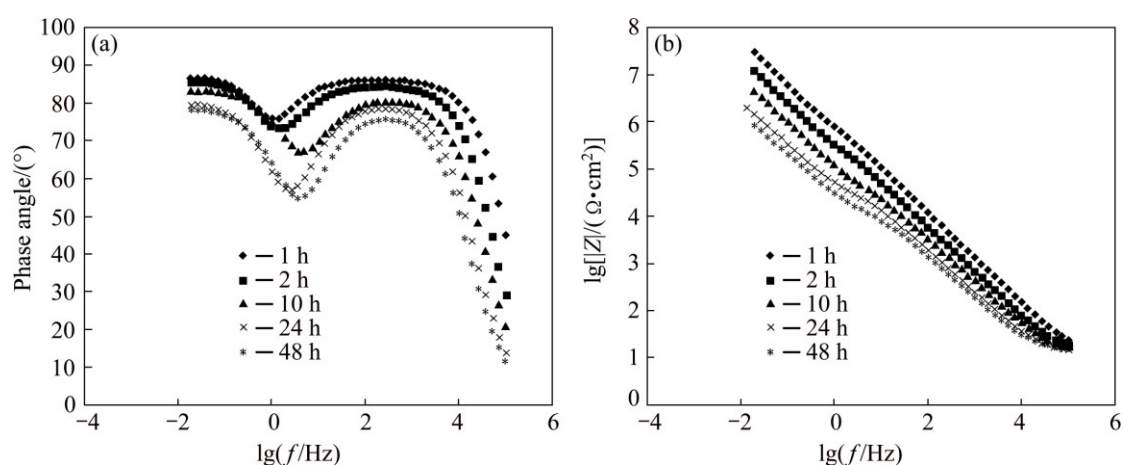
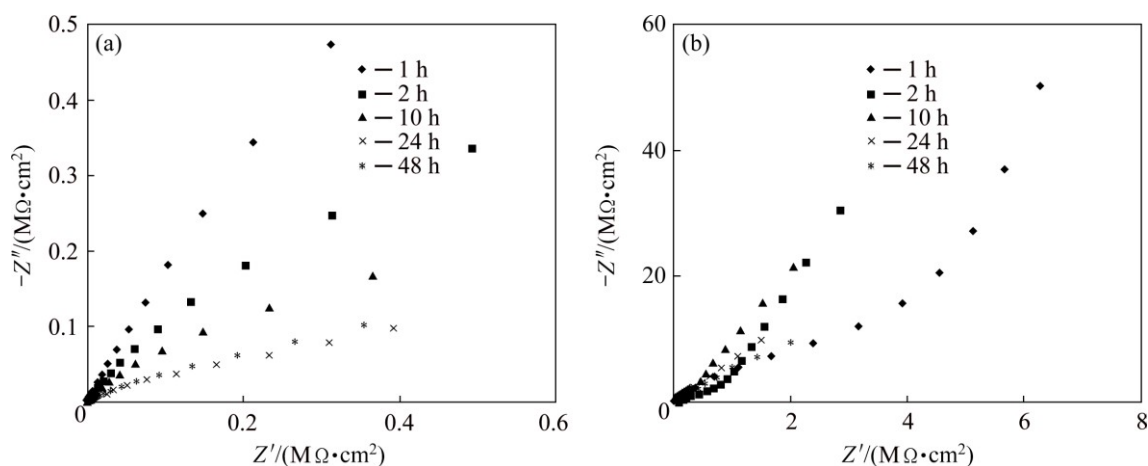
The Bode phase and Bode magnitude plots after immersion testing of the boiling-water-sealed-anodised alloys are also shown in Figs. 7(a) and (b), respectively. Decrease in $|Z|$ and in phase angle by immersion time indicates the evolution of impedance parameters.

The same immersion process has done for the stearic acid sealed anodised samples and EIS measurements were also carried out after immersion. The related Nyquist plots are shown in Fig. 8 and the resulted EIS parameters are reported in Table 6. Furthermore, the resulted Bode phase and Bode magnitude plots are also shown in Fig. 9.

Pit initiation and growth on the alloy surface means electrolyte penetration through the barrier layer and if this happens, a third time constant would appear in the spectra. Therefore, a new parameter of R_{corr} and double layer constant phase element (CPE_{dl}) should be introduced in the equivalent circuit. By considering the

Table 6 EIS parameters of porous and barrier layer after immersion testing for sealed-anodised alloy

Sealant	Immersion time/h	$C_1/(\mu\text{F}\cdot\text{cm}^2)$	$C_2/(\mu\text{F}\cdot\text{cm}^2)$	$R_1/(\Omega\cdot\text{cm}^2)$	$R_2/(\Omega\cdot\text{cm}^2)$	n_1	n_2
Boiling water	1	0.25	0.21	3×10^5	1.4×10^9	0.93	0.98
	2	0.48	0.42	1×10^5	1.4×10^9	0.92	0.96
	10	0.67	0.79	2×10^4	1×10^9	0.89	0.93
	24	0.91	1.73	2×10^4	1×10^8	0.89	0.90
	48	1.14	2.31	9×10^3	1×10^8	0.87	0.88
Molten stearic acid	1	0.22	0.18	4.8×10^6	2.1×10^{10}	0.95	0.98
	2	0.28	0.23	8×10^5	6.7×10^9	0.95	0.96
	10	0.41	0.29	2×10^5	3×10^9	0.95	0.95
	24	0.59	0.38	4×10^4	2×10^9	0.93	0.91
	48	0.76	0.61	4×10^4	2×10^8	0.92	0.90

**Fig. 7** EIS results after immersion testing for anodised samples sealed in boiling water: (a) Bode phase plots; (b) Bode magnitude plots**Fig. 8** Nyquist plots after immersion testing for anodised sample sealed in molten stearic acid: (a) High and medium frequency range corresponding to porous layer; (b) Low frequency range corresponding to barrier layer

resulted Nyquist and Bode plots for the sealed alloys, it can be seen that third time constant did not appeared in the spectra which indicated that corrosion did not happen even after 48 h of immersion.

By considering the resulted EIS parameters in Table 6, the evolution of capacitive behaviour of the porous and barrier layers with time is compared in Figs. 10(a)

and (b), respectively. It is obvious that the rate of increase in the capacitive behaviour of the layers is less in the case of sealing in molten stearic acid. Thus, sealing in molten stearic acid provides more corrosion resistance and durability in comparison with boiling water. As it was mentioned before, this is due to the hydrophobicity of aluminium-soap phase which formed

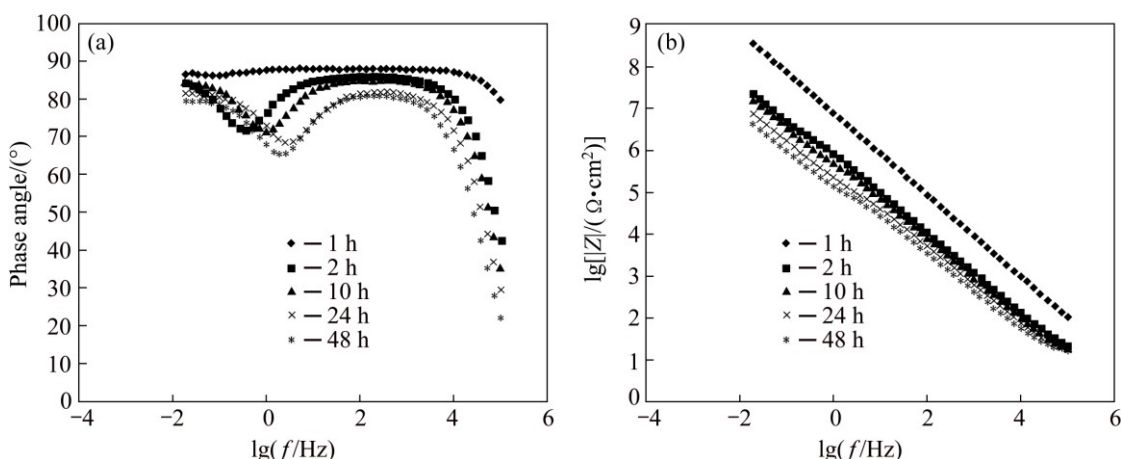


Fig. 9 EIS results after immersion testing for anodised samples sealed in molten stearic acid: (a) Bode phase plots; (b) Bode magnitude plots

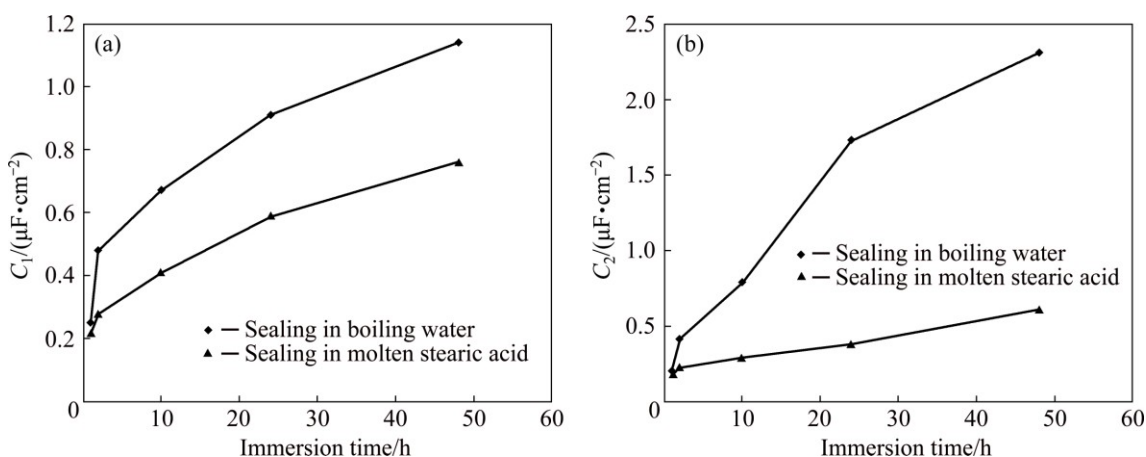


Fig. 10 Change in capacitive behaviour of porous layer (a) and barrier layer (b) with immersion time

during sealing in molten stearic acid [12]. Both of the immersed alloys have a reasonable amount of capacitance, resistance and *n* values even after 48 h of immersion compared with similar works [9], implying that our method provides reasonable corrosion resistance and durability for 2024-T3 alloy.

Salt spray test was performed on the sealed and unsealed samples according to ASTM B117. Corrosion resistance of the investigated materials was studied during salt spray technique by monitoring the onset of appearing corrosion spots on the samples every 24 h. The results of the salt spray test are reported in Table 7. The corrosion spots appeared on the surface of the unsealed oxide layer after 288 h; while it appeared after 336 and 480 h of exposure for the samples sealed in boiling water and molten stearic acid, respectively. This indicates the excellent corrosion resistance of the oxide layer sealed in molten stearic acid.

3.2.6 Effect of cerium ion on growth rate of barrier layer

In order to investigate the effect of cerium ion on the growth rate of the barrier layer, the alloys were anodised in the mixed acid electrolyte with and without

Table 7 Results of salt spray test for anodised samples

Anodised sample	Time/h
Unsealed	288
Sealed in boiling water	336
Sealed in molten stearic acid	480

0.1 mol/L cerium sulphate salt. Anodising was performed for 5, 10 and 20 min. All of the anodised alloys were sealed in boiling water for 30 min. The thicknesses of the barrier layers were determined by Eq. (2) and the results are shown in Fig. 11. It is apparent from the figure that the thickness of the barrier layer increases linearly with time up to 20 min. But the thickening rate of the oxide layer grown in electrolyte containing cerium ion is higher than that of the oxide layer grown in electrolyte without cerium ion. It can be concluded that adding cerium inhibitor to the anodising electrolyte could effectively increase the rate of oxide film growth by double. This is due to the high oxidizing power of cerium.

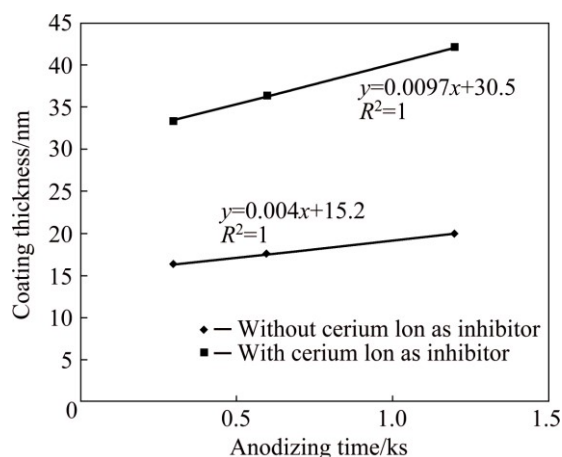


Fig. 11 Rate of thickening of barrier layer in case of anodising in presence and absence of cerium ion in electrolytes

4 Conclusions

1) The anodising process of 2024-T3 aluminum alloy was performed in a new electrolyte of sulfuric/boric/phosphoric mixed acid containing 0.1 mol/L cerium sulfate as a corrosion inhibitor, which was found to be an effective method to improve the corrosion resistance of the 2024 aluminum alloy. A homogeneous alumina coating was obtained and sealing in molten stearic acid resulted in increase in corrosion resistance and durability of the oxide layer. The results of salt spray tests were in good agreement with EIS measurements indicating excellent corrosion performance of the sealed anodised alloys.

2) The cerium ion in anodising electrolyte was acted as a cathodic inhibitor and led to increase in the homogeneity of the oxide coating and also thickness of the barrier oxide layer owing to high oxidizing power of cerium ion. It can be concluded that adding cerium inhibitor to the anodising electrolyte could effectively increase the rate of oxide film growth leading to more corrosion resistance of the anodic oxide film.

3) The optimum corrosion resistant for 2024-T3 aluminium alloy was obtained by anodising via the following procedure: immersion of the alloy in the mixed acid containing 0.1 mol/L cerium sulphate salt for 1800 s then anodising for 20 min under the current density of 1 mA/cm² followed by sealing in molten stearic acid for 30 min.

References

- HELLER DAIMON K, FAHRENHOLTZ WILLIAM G, O'KEEFE MATTHEW J. The effect of post treatment time and temperature on cerium-based conversion coatings on Al 2024-T3 [J]. *Corrosion Science*, 2010, 52: 360–368.
- GARCÍA S J, MUSTER T H, ÖZKANAT Ö, SHERMAN N, HUGHES A E, TERRY N H, DE WIT J, MOL J M C. The influence of pH on corrosion inhibitor selection for 2024-T3 aluminium alloy assessed by high-throughput multielectrode and potentiodynamic testing [J]. *Electrochimica Acta*, 2010, 55: 2457–2465.
- SAEEDIKHANI M, JAVIDI M, YAZDANI A. Anodizing of 2024-T3 aluminum alloy in sulfuric-boric-phosphoric acids and its corrosion behavior [J]. *Transactions of Nonferrous Metals Society of China*, 2013, 23: 2551–2559.
- MASON R B, CLARK S, KLINGENBERG M, MILLER M, BERMAN E, VOEVODIN N. Type II anodizing operations: Test results hold promise for alternatives to dichromate sealer [J]. *Metal Finishing*, 2012, 110: 11–18.
- CAPELOSSI V, POELMAN M, RECLOUX I, HERNANDEZ R, de MELO H, OLIVIER M G. Corrosion protection of clad 2024 aluminum alloy anodized in tartaric-sulfuric acid bath and protected with hybrid sol-gel coating [J]. *Electrochimica Acta*, 2014, 124: 69–79.
- WANG Jia-yu, LI Cheng, ZHENG Shum-li, YIN Cheng-yong, WANG Yan-hui. Growth and corrosion behaviors of thin anodic alumina membrane on AA5083 Al–Mg alloy in incandescent medium [J]. *Transactions of Nonferrous Metals Society of China*, 2014, 24: 3023–3030.
- MOUTARLIER V, GIGANDET M, RICQ L, PAGETTI J. Electrochemical characterisation of anodic oxidation films formed in presence of corrosion inhibitors [J]. *Applied Surface Science*, 2001, 183: 1–9.
- MOUTARLIER V, GIGANDET M, PAGETTI J, NORMAND B. An electrochemical approach to the anodic oxidation of Al 2024 alloy in sulfuric acid containing inhibitors [J]. *Surface and Coatings Technology*, 2002, 161: 267–274.
- MOUTARLIER V, GIGANDET M, NORMAND B, PAGETTI J. EIS characterisation of anodic films formed on 2024 aluminium alloy in sulphuric acid containing molybdate or permanganate species [J]. *Corrosion Science*, 2005, 47: 937–951.
- TANG Jun-lei, HAN Zhong-zhi, ZUO Yu, TANG Yu-ming. A corrosion resistant cerium oxide based coating on aluminum alloy 2024 prepared by brush plating [J]. *Applied Surface Science*, 2011, 257: 2806–2812.
- YU Xing-wen, CAO Chu-nan. Electrochemical study of the corrosion behavior of Ce sealing of anodized 2024 aluminum alloy [J]. *Thin Solid Films*, 2003, 423: 252–256.
- ZUO Yu, ZHAO Peng-hui, ZHAO Jing-mao. The influences of sealing methods on corrosion behavior of anodized aluminum alloys in NaCl solutions [J]. *Surface and Coatings Technology*, 2003, 166: 237–242.
- LIU Wen-yong, LUO Yu-ting, SUN Lin-yu, WU Ruo-mei, JIANG Hai-yun, LIU Yue-jun. Fabrication of the superhydrophobic surface on aluminum alloy by anodizing and polymeric coating [J]. *Applied Surface Science*, 2013, 264: 872–878.
- HERRERA-HERNANDEZ H, VARGAS-GARCIA J, HALLEN-LOPEZ J, MANSFELD F. Evaluation of different sealing methods for anodized aluminum–silicon carbide (Al/SiC) composites using EIS and SEM techniques [J]. *Materials and Corrosion*, 2007, 58: 825–832.
- HUANG Yue-long, SHIH Hong, HUANG Huo-chuan, DAUGHERTY J, WU Shun, RAMANATHAN S, CHANG C, MANSFELD F. Evaluation of the corrosion resistance of anodized aluminum 6061 using electrochemical impedance spectroscopy (EIS) [J]. *Corrosion Science*, 2008, 50: 3569–3575.
- SHI Hong-wei, HAN En-hou, LAMAKA S V, ZHELUDKEVICH M L, LIU Fu-chun, FERREIRA M G S. Cerium cinnamate as an environmentally benign inhibitor pigment for epoxy coatings on AA 2024-T3 [J]. *Progress in Organic Coatings*, 2014, 77: 765–773.
- HUA Tian-hui, SHI Hong-wei, WEI Tao, LIU Fu-chun, FAN Shi-hua, HAN En-Hou. Cerium tartrate as a corrosion inhibitor for AA

- 2024-T3 [J]. Corrosion Science, 2015, 95: 152–161.
- [18] HSU C, MANSFELD F. Technical note: Concerning the conversion of the constant phase element parameter Y_0 into a capacitance [J]. Corrosion, 2001, 57: 747–748.
- [19] HUANG Y, SHIH H, MANSFELD F. Concerning the use of constant phase elements (CPEs) in the analysis of impedance data [J]. Materials and Corrosion, 2010, 61: 302–305.
- [20] YASAKAU KIRYL A, ZHELUDKEVICH MIKHAIL L, LAMAKA SVIATLANA V, FERREIRA MARIO G S. Mechanism of corrosion inhibition of AA2024 by rare-earth compounds [J]. Physical Chemistry B, 2006, 110: 5515–5528.
- [21] DABALÀ M, RAMOUS E, MAGRINI M. Corrosion resistance of cerium-based chemical conversion coatings on AA5083 aluminium alloy [J]. Materials and Corrosion, 2004, 55: 381–386.

2024-T3 铝合金在含铈盐缓蚀剂 硫酸–硼酸–磷酸混合酸中的阳极氧化

Mohsen SAEEDIKHANI¹, Mehdi JAVIDI², Sareh VAFAKHAH³

Department of Materials Science and Engineering, School of Engineering,
Shiraz University, Zand Street, Shiraz 7134851154, Iran

摘要: 研究了铈盐缓蚀剂对 2024-T3 铝合金阳极氧化的影响。采用带 X 射线能谱仪的扫描电子显微镜分析合金表面处理前后的表面组分。使用含 0.1 mol/L 硫酸铈盐的混合电解液作为阳极氧化电解液, 该混合电解液由 10% 硫酸、5% 硼酸和 2% 磷酸组成。在沸水和溶化的硬脂酸中进行密封处理, 分别利用电化学交流阻抗和盐雾技术研究氧化膜的腐蚀行为和耐用性。结果表明, 阳极氧化电解液中存在的铈离子导致合金更均匀, 氧化膜生长率提高和氧化层的厚度增加, 这些都是因为铈离子具有高的氧化能力。

关键词: 铝合金; 阳极氧化; 混合酸; 铈盐; 缓蚀剂

(Edited by Xiang-qun LI)